

The Through-Plane Problem for Tagged MR Images

Delman Lee*, John T. Kent* and Kanti V. Mardia*

Abstract

An iterative algorithm is proposed to recover the 3D deformation of the heart wall from tagged magnetic resonance (MR) images. Tagged MR images provide limited information about the deformation due to the “through-plane problem”. The proposed method provides exact estimates of the parameters of the through-plane problem. The deformation is recovered by minimizing an objective function which penalizes (i) the roughness of the deformation, plus (ii) the discrepancy between the observed data and the fitted deformation.

1 The Through-Plane Problem

A non-invasive technique for monitoring the deformation of the heart wall is tagged Magnetic Resonance (MR) imaging [1, 2]. Tagged MR images are acquired at an imaging plane fixed in 3D space. However, during data acquisition the heart moves through the imaging plane and leads to the so called *through-plane problem*. The problem is best illustrated by its 2D analogue.

The left hand two pictures of Fig. 1 show a deformation in 2D. A set of vertical lines at time 0 are deformed to curves at time t . In a conventional setting, labelled points on the lines/curves are observed before and after deformation. However, in the through-plane problem, the observations consist of the intersections of the curves with the (horizontal) imaging lines before and after deformation. For example in Fig. 1, we have a horizontal data set, where one can only observe the displacement of the intersections of the “vertical” curves (solid line) with the horizontal imaging lines (dashed line). We termed the points such as $\mathbf{x}_{i_p}^0$ and $\mathbf{x}_{i_p}^t$ the observed *intersection landmarks*. We have similar observations for a vertical data set. The aim is to recover the underlying deformation from the displacements of horizontal and vertical intersection landmarks. For the 3D problem in tagged MR images, data are acquired at imaging planes instead of imaging lines, and observations can be reduced to the intersections of curves with the imaging planes. Similar problems have been tackled by [3, 4].

A common acquisition of tagged MR images consist of 2-3 sets of parallel imaging planes, at approximately orthogonal directions, and ~ 500 intersection landmarks. Each set of parallel imaging planes consist of 5-10 imaging planes.

Notations We shall present our algorithm for the 3D problem, where column vectors are denoted by bold lower-case italic letters. Let there be P imaging planes $\{\pi_p\}_{p=1}^P$, and L parametric lines $\{\mathbf{x}_l(u)\}_{l=1}^L$. An imaging plane π_p is given by $\mathbf{n}_p^T \mathbf{x} = k_p$, where \mathbf{n}_p is the normal vector and k_p the offset. A parametric line $\mathbf{x}_l(u)$ is described by a starting point $\boldsymbol{\nu}_l$ and a tangent vector \mathbf{n}_l , i.e. $\mathbf{x}_l(u) = \boldsymbol{\nu}_l + u \mathbf{n}_l$. A parametric line is typically normal to an imaging plane π_p so that $\mathbf{n}_l = \mathbf{n}_p$ for some p . Let $\mathbf{f}^t : \mathbb{R}^3 \rightarrow \mathbb{R}^3$ denote the deformation between time 0 and time t . The data at time t consists of observed intersection landmarks $\mathbf{x}_{i_p}^t$, which are the intersections of the curves $\mathbf{f}^t(\mathbf{x}_l(\cdot))$ with the imaging planes π_p , i.e. $\mathbf{x}_{i_p}^t = \mathbf{f}^t(\mathbf{x}_l(u_{i_p}))$ where u_{i_p} satisfies $\mathbf{n}_p^T \mathbf{f}^t(\mathbf{x}_l(u_{i_p})) = k_p$. Let \mathcal{I} denotes the set of intersection landmarks indexed by the pair (l, p) .

2 Solutions

A deformation $\mathbf{f} : \mathbb{R}^3 \rightarrow \mathbb{R}^3$ is modelled as a set of three spline functions: $\mathbf{f}(\mathbf{x}) = (f_1(\mathbf{x}) \ f_2(\mathbf{x}) \ f_3(\mathbf{x}))^T$, where the superscript T denote transposition. Our choice for the space of spline functions is spanned by the tensor product of cubic B-splines. Let there be K equi-spaced knots with spacing Δ in each dimension. The dimension of this space of spline functions is $N = (K + 2)^3$. The extra two degrees of freedom for each dimension arises because our splines are not constrained by any boundary conditions. For details see e.g. [5]. Note that deformation

*Email: {delman.john,sta6kvm}@amsta.leeds.ac.uk Post: Department of Statistics, University of Leeds, Leeds, LS2 9JT, U.K..

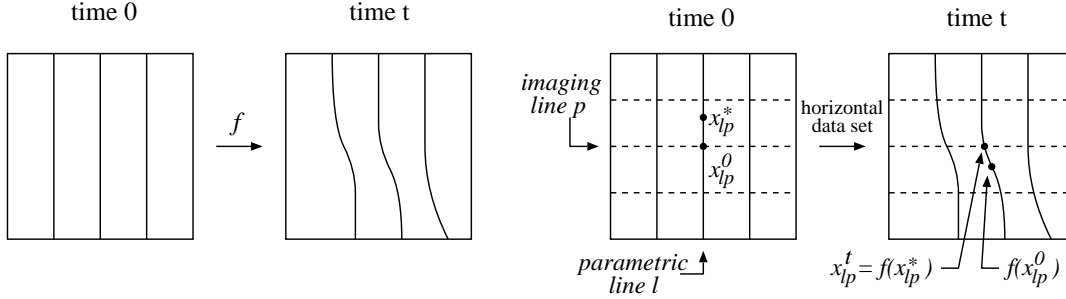


Figure 1: Description of the intersection landmarks \mathbf{x}_{lp}^0 and \mathbf{x}_{lp}^t . \mathbf{f} is the underlying deformation. Dashed lines are the imaging lines. Solid curves are the parametric curves.

using a set of tensor product of cubic B-splines is used to construct the “B-solid” of [6]. A deformation $\mathbf{f}(\mathbf{x})$ can be written in matrix form as:

$$\mathbf{f}(\mathbf{x}) = C^T \mathbf{b}(\mathbf{x}), \quad (1)$$

where $\mathbf{b}(\mathbf{x})$ is an N -dimensional vector of basis functions, \mathbf{c}_d is an N -dimensional vector of coefficients for the d th spline function ($d=1, 2, 3$), and $C = (\mathbf{c}_1 \mathbf{c}_2 \mathbf{c}_3)$ is an $N \times 3$ matrix of all coefficients.

The roughness of a deformation \mathbf{f} is measured by the sum of the thin-plate roughness penalties $\sum_{d=1}^3 J(f_d)$, where

$$J(f_d) = \int_{\Omega} \sum_{i,j=1}^3 \left(\frac{\partial^2 f_d}{\partial x_i \partial x_j} \right)^2 d\mathbf{x} = \mathbf{c}_d^T K \mathbf{c}_d, \quad (2)$$

and Ω is the rectangular region of integration, and K is an $N \times N$ matrix. For a tensor product of cubic B-splines, the matrix K is sparse. We chose the tensor product of cubic B-splines for computational reasons. The above framework also applies to other types of splines and basis functions (see e.g. [7]).

For each time t , we construct a deformation \mathbf{f}^t that minimizes the sum of two terms: (i) a roughness penalty on the deformation, and (ii) a discrepancy term which measures the difference between the observed intersection landmark \mathbf{x}_{lp}^t and the intersection landmark of the deformation \mathbf{f}^t . The optimization is done by the conjugate gradient method which requires the derivatives of the objective function.

2.1 Approximate Solution

Dropping the superscript t on \mathbf{f}^t , consider the following objective function, which is invariant to scale changes in the coordinates:

$$\phi_0(C) = \frac{\lambda}{2\Omega} \sum_{d=1}^3 \mathbf{c}_d^T K \mathbf{c}_d + \frac{1}{2M\Delta^2} \sum_{(l,p) \in \mathcal{I}} \| Q_p [\mathbf{f}(\mathbf{x}_{lp}^0) - \mathbf{x}_{lp}^t] \|^2 \quad (3)$$

where M is the number of intersection landmarks in \mathcal{I} , $Q_p = I - \mathbf{n}_p \mathbf{n}_p^T / (\mathbf{n}_p^T \mathbf{n}_p)$ is the orthogonal projection matrix onto the plane going through the origin and parallel to the imaging plane π_p , and λ is a weight which controls the relative importance of the two terms. The first term in (3) is the roughness penalty, while the second term is the discrepancy between the observed intersection landmark \mathbf{x}_{lp}^t and an approximation to the intersection landmark of the deformation \mathbf{f} . The approximation is exact for deformations which consist of a translation and a scale change, but not otherwise. For example, in Fig. 1, the orthogonal projection of $\mathbf{f}(\mathbf{x}_{lp}^0)$ onto the imaging line p is far away from the true intersection landmark \mathbf{x}_{lp}^t of the deformation. The term $Q_p [\mathbf{f}(\mathbf{x}_{lp}^0) - \mathbf{x}_{lp}^t]$ in (3) is the same as the “force” on the deformable model of [8]. The objective function in (3) is quadratic in C with derivatives linear in C given by

$$\nabla_{\mathbf{c}_d} \phi_0 = \frac{\lambda}{\Omega} K \mathbf{c}_d + \frac{1}{M\Delta^2} \sum_{(l,p) \in \mathcal{I}} (\nabla_{\mathbf{c}_d} \mathbf{f}^T) Q_p [\mathbf{f}(\mathbf{x}_{lp}^0) - \mathbf{x}_{lp}^t] \quad (4)$$

for $d=1, 2, 3$. The derivative $\nabla_{c_d} \mathbf{f}^T$, evaluated at $\mathbf{x}=\mathbf{x}_{lp}^0$, is an $N \times 3$ matrix where the d th column is $\mathbf{b}(\mathbf{x})$ and all other columns are zero. It can be shown that if each image plane is perpendicular to one of the coordinate axes, then (4) becomes a decoupled system of equations, where the coefficients for each dimension can be solved separately. However, this is not typically true in practice. e.g. the ‘‘fan’’ of imaging planes of [9].

The minimum of (3) can be regarded as the ‘‘zeroth-order’’ solution, where we approximate an intersection landmark of the deformation \mathbf{f} by orthogonal projection onto the imaging plane π_p . A ‘‘first-order’’ solution is to use the tangent direction of the deformed curve at \mathbf{x}_{lp}^0 to arrive at a better approximation of the intersection landmark. The first-order approximation is exact under any affine deformation. However, in the next section, we shall present the general exact solution which imposes only a minor extra computational burden over the first-order solution.

2.2 Exact Solution

Dropping the superscript t on \mathbf{f}^t , consider the objective function:

$$\phi(C) = \frac{\lambda}{2\Omega} \sum_{d=1}^3 c_d^T K c_d + \frac{1}{2M\Delta^2} \sum_{(l,p) \in \mathcal{I}} \|\mathbf{f}(\mathbf{x}_l(u_{lp})) - \mathbf{x}_{lp}^t\|^2 \quad (5)$$

where u_{lp} satisfies $\mathbf{n}_p^T \mathbf{f}(\mathbf{x}_l(u_{lp})) = k_p$. Using the implicit function theorem, it can be verified that the derivative of (5) is given by

$$\nabla_{c_d} \phi = \frac{\lambda}{\Omega} K c_d + \frac{1}{M\Delta^2} \sum_{(l,p) \in \mathcal{I}} (\nabla_{c_d} \mathbf{f}^T) R_{lp}^T [\mathbf{f}(\mathbf{x}_l(u_{lp})) - \mathbf{x}_{lp}^t] \quad (6)$$

for $d=1, 2, 3$, where

$$R_{lp} = I - \frac{(\nabla_{\mathbf{x}} \mathbf{f}^T)^T \mathbf{n}_l \mathbf{n}_p^T}{\mathbf{n}_p^T (\nabla_{\mathbf{x}} \mathbf{f}^T)^T \mathbf{n}_l}. \quad (7)$$

The derivatives $\nabla_{c_d} \mathbf{f}^T$ and $\nabla_{\mathbf{x}} \mathbf{f}^T$ are evaluated at $\mathbf{x}=\mathbf{x}_l(u_{lp})$. For a given deformation \mathbf{f} , the parameter u_{lp} can be computed by the Newton-Raphson method on $\mathbf{n}_p^T \mathbf{f}(\mathbf{x}_l(u_{lp})) = k_p$.

The derivative of the approximate intersection landmark $Q_p \mathbf{f}(\mathbf{x}_{lp}^0)$ in (3) with respect to the coefficient c_d is the orthogonal projection of the derivative of the point $\mathbf{f}(\mathbf{x}_{lp}^0)$ onto the imaging plane π_p , i.e. the transpose of $(\nabla_{c_d} \mathbf{f}^T) Q_p$ in (4). Similarly, the derivative of the exact intersection landmark $\mathbf{f}(\mathbf{x}_l(u_{lp}))$ in (5) with respect to the coefficient c_d is given by an oblique projection of the derivative of the point $\mathbf{f}(\mathbf{x}_l(u_{lp}))$ onto the imaging plane π_p , i.e. the transpose of $(\nabla_{c_d} \mathbf{f}^T) R_{lp}^T$ in (6). Note that $(\nabla_{\mathbf{x}} \mathbf{f}^T)^T \mathbf{n}_l$ is the tangent direction of the curve $\mathbf{f}(\mathbf{x}_l(\cdot))$ at $u=u_{lp}$. Treating $\mathbf{x}_l(u_{lp})$ as the origin, R_{lp} is the oblique projection, parallel to the tangent direction $(\nabla_{\mathbf{x}} \mathbf{f}^T)^T \mathbf{n}_l$, onto the imaging plane π_p .

3 Results & Discussion

Results for a clinical data set will be presented at the meeting. The data set consists of images of the left ventricle of patients before and after surgery. The aim is to determine the success of the surgery. For illustrative purposes, we present a two-pass algorithm on a 2D deformation here. The first and second passes are, respectively, the iterative optimization procedures in § 2.1 and § 2.2. The output of the first pass is the input to the second pass. The algorithm is best illustrated here with a 2D deformation. Fig. 2 shows a 2D deformation and the results of the two passes (with $\lambda=0.01$) on a data set with $L=8$ (2 orthogonal sets of 4) parametric lines, $P=8$ (2 orthogonal sets of 4) imaging lines and 32 intersection landmarks. Note the substantial difference between the zeroth-order solution and the exact solution around the point X in Fig. 2. The algorithm have also been tested on a simulated 3D data set with $L=32$ (2 orthogonal sets of 16) parametric lines, $P=8$ (2 orthogonal sets of 4) imaging planes and 128 intersection landmarks. Using $\lambda=0.01$, we achieved an average discrepancy (second term in (5)) of 0.1%. The computational time for each frame took approximately 1.5min(1st pass)+2.5min(2nd pass) on a Sun UltraSPARC.

A major consideration in solving the through-plane problem in 3D is the computational speed of the method. The tensor product of cubic B-splines is chosen due to the ease of computing the value and derivatives of the deformation, both of which require a constant number of operations irrespective of the total number of basis functions.

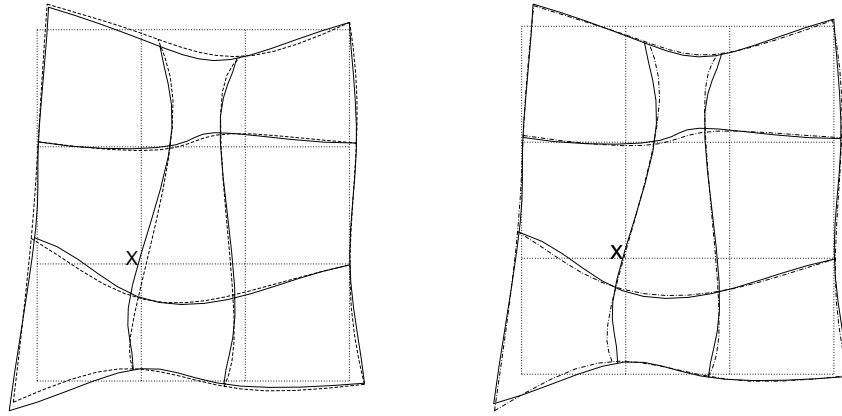


Figure 2: *Left*: Approximate solution (dashed line). *Right*: Exact solution (dot-dashed line). *Dotted line*: Imaging lines. *Solid line*: Underlying deformation.

Optimization is done by the conjugate gradient method, whose convergence rate may be improved by an appropriate variable transformation, termed *preconditioning*. The time to convergence of an iterative procedure also relies on how close the current iterate is to the answer. This opens up many possibilities for improving the speed of the method by successive approximations to the answer. For example, a hierarchical system of incorporating the intersection landmarks, where only a sparse subset of the intersection landmarks is used at the initial stages of the algorithm. Another possibility is a multi-resolution scheme, where one solves the problem for a small number of basis functions in the initial stage of the algorithm and gradually builds up to the full set of basis functions.

We have parameterized the 3D deformation in cartesian coordinates. Alternative parameterizations like those in [6, 8] can be incorporated into the current method.

References

- [1] Zerhouni, E., Parish, D., Rogers, W., Yang, A., and Shapiro, E. *Radiology* **169**, 59–63 (1988).
- [2] Axel, L. and Dougherty, L. *Radiology* **172**, 349–350 (1989).
- [3] Bookstein, F. In *Proceedings in Image Fusion and Shape Variability Techniques*, Mardia, K., Gill, C., and Dryden, I., editors, 59–70. Leeds University Press, (1996).
- [4] Green, W. In *Proceedings in Image Fusion and Shape Variability Techniques*, Mardia, K., Gill, C., and Dryden, I., editors, 79–87. Leeds University Press, (1996).
- [5] Green, P. and Silverman, B. *Nonparametric Regression and Generalized Linear Models*. Chapman & Hall, London, (1994).
- [6] Radeva, P., Amini, A., Huang, J., and Martí, E. In *Proceedings of the IEEE Workshop on Mathematical Methods in Biomedical Image Analysis*, 192–201, June (1996).
- [7] Kent, J. and Mardia, K. In *Probability, Statistics and Optimisation*, Kelly, F., editor, chapter 24, 325–339. John Wiley, New York (1994).
- [8] Park, J., Metaxas, D., and Axel, L. *Medical Image Analysis* **1**(1), 53–71 (1996).
- [9] O’Dell, W., Moore, C., W.C., H., Zerhouni, E., and McVeigh, E. *Radiology* **195**(3), 829–835 June (1995).

Acknowledgment: The work is supported under the EPSRC Stochastic Modelling in Science and Technology programme. We would like to thank Liz Berry, Bill Crum, John Ridgway and U. Sivanathan for useful discussions and for providing us with the data set.